INSTITUTE OF PHYSICS PUBLISHING PHYSICS IN MEDICINE AND BIOLOGY

Phys. Med. Biol. **49** (2004) 3117–3124 PII: S0031-9155(04)79427-0

Photoacoustic imaging with deconvolution algorithm

Yi Wang, Da Xing[1], Yaguang Zeng and Qun Chen

Institute of Laser Life Science, South China Normal University, Guangzhou 510631, People's Republic of China

E-mail: xingda@scnu.edu.cn

Received 16 April 2004
Published 28 June 2004
Online at stacks.iop.org/PMB/49/3117
doi:10.1088/0031-9155/49/14/006

Abstract

The impulse response of the ultrasonic transducer used for detection is crucial for photoacoustic imaging with high resolution. We demonstrate a reconstruction method that allows the optical absorption distribution of a sample to be reconstructed without knowing the impulse response of the ultrasonic transducer. A convolution relationship between photoacoustic signals measured by an ultrasound transducer and optical absorption distribution is developed. Based on this theory, the projection of the optical absorption distribution of a sample can be obtained directly by deconvolving the recorded PA signal originating from a point source out of that from the sample. And a modified filtered back projection algorithm is used to reconstruct the optical absorption distribution. We constructed a photoacoustic imaging system to validate the reconstruction method and the experimental results demonstrated that the reconstructed images agreed well with the original phantom samples. The spatial resolution of the system reaches 0.3 mm.

1. Introduction

Photoacoustic (PA) imaging is a novel imaging technique that combines the advantages of pure optical imaging and pure ultrasound imaging. In the past decade, a number of papers describing PA imaging techniques have been presented (Esenaliev *et al* 1999, Kruger *et al* 1995, Oraevsky *et al* 1999, Wang *et al* 2003). Various PA imaging algorithms have been developed, such as the 3D inverse Radon transform (Kruger *et al* 1999), and the modified back-projection algorithm (Xu and Wang 2002), etc. With these algorithms, the impulse response of the ultrasonic transducer used for detection is crucial for PA imaging with high resolution, and it is required for calculating induced PA pressures. The impulse response of an acoustic transducer is the response of the transducer when the input acoustic wave

[1] Author to whom correspondence should be addressed.

can be approximated as a temporal delta function. And the measured PA signals are the convolutions of induced PA pressures and the impulse response. It was suggested that the impulse response could be measured by illuminating the transducer with a weak laser pulse (Kruger *et al* 1999, Xu and Wang 2002). Practically, this method is not appropriate because the 'impulse response' measured according to this method is the convolution of the PA pressure produced on the surface of the transducer and the exact impulse response of the transducer, and in addition, it is also partially dependent on the shape of the irradiating laser pulse.

Tomographic imaging deals with reconstructing an image from its projections. A projection is the integral of the image in a specified direction. In this paper, we deduce a convolution relationship between PA signals recorded by an ultrasound transducer and optical absorption distribution. Based on this relationship, the projection of the optical absorption distribution of a sample is obtained directly by deconvolving the recorded PA signal originating from a point source out of that from the sample. PA signals from a point source can be easily measured by focusing the incident laser on an absorber surface to form a point source. The approach allows the optical absorption distribution to be reconstructed without knowing the impulse response of the transducer.

2. Theory

To induce the PA effect, the PA pressure produced by the heat source $H(\mathbf{r}, t)$ obeys the following equation (Kruger *et al* 1995, Xu and Wang 2002):

$$\nabla^2 p(\mathbf{r}, t) - \frac{1}{c^2}\frac{\partial^2}{\partial t^2} p(\mathbf{r}, t) = -\frac{\beta}{C_p}\frac{\partial}{\partial t} H(\mathbf{r}, t) \tag{1}$$

where β is the isobaric volume expansion coefficient, c is the sound speed and C_p is the specific heat. For convenience, we choose the transducer position as the origin of the coordinates, so the PA pressure at transducer position and time t can be expressed as (Kruger *et al* 1995, Xu and Wang 2002)

$$p(t) = \frac{\beta}{4\pi C_p} \int\int\int \frac{\mathrm{d}\mathbf{r}}{r} \frac{\partial H(\mathbf{r}, t')}{\partial t'}\bigg|_{t'=t-\frac{r}{c}} \tag{2}$$

where $r = |\mathbf{r}|$. $H(\mathbf{r}, t)$ can be expressed as $H(\mathbf{r}, t) = A(\mathbf{r})I(t)$, where $A(\mathbf{r})$ is the spatial absorption distribution and $I(t)$ is the temporal illumination function. Equation (2) can be written as

$$p(t) = \frac{\beta}{4\pi C_p} \int\int\int \frac{\mathrm{d}\mathbf{r}}{r} A(\mathbf{r}) I'\left(t - \frac{r}{c}\right) \tag{3}$$

where $I'(t) = \mathrm{d}I(t)/\mathrm{d}t$. In spherical coordinates, we can write

$$p(t) = \frac{\beta}{4\pi C_p} \int \left(\frac{1}{r}\int\int A(r, \theta, \phi) r^2 \sin\theta \,\mathrm{d}\theta \,\mathrm{d}\phi\right) I'\left(t - \frac{r}{c}\right) \mathrm{d}r. \tag{4}$$

Assuming $t' = r/c$, equation (4) can be written as

$$\begin{aligned} p(t) &= \frac{\beta}{4\pi C_p} \int \left(\frac{1}{t'}\int\int A(ct', \theta, \phi)(ct')^2 \sin\theta \,\mathrm{d}\theta \,\mathrm{d}\phi\right) I'(t - t') \,\mathrm{d}t' \\ &= \frac{\beta}{4\pi C_p} \left(\frac{1}{t} \oint\int_{|\mathbf{r}|=ct} A(\mathbf{r}) \,\mathrm{d}S\right) * I'(t) \end{aligned} \tag{5}$$

where the asterisk denotes convolution operation. Additionally, the PA pressure produced by a point source with the same temporal illumination function $I(t)$ as above can be expressed as (Callasso *et al* 2001)

$$p_p(t) = k\frac{1}{r_p}I'\left(t - \frac{r_p}{c}\right) \tag{6}$$

where $I'(t) = \mathrm{d}I(t)/\mathrm{d}t$, r_p is the distance between the point source and the field point and k is a parameter depending on the absorption property of the point source and the parameters of the irradiating light. Let $p_0(t) = p_p(t + r_p/c) = kI'(t)/r_p$, i.e., $p_0(t)$ denotes the PA pressure from the point source with a delay time of $-r_p c$. Thus, from equation (5) we get

$$p(t) = \frac{\beta r_p}{4\pi C_p k}\left(\frac{1}{t}\oint\int_{|\mathbf{r}|=ct} A(\mathbf{r})\,\mathrm{d}S\right) * p_0(t). \tag{7}$$

In equation (7), the term $\oint\int_{|\mathbf{r}|=ct} A(\mathbf{r})\,\mathrm{d}S$ is the 'projections' of the optical absorption distribution over spherical surfaces. Equation (7) indicates that an absorber can be separated into a collection of point sources and the PA pressures from the heat source are the linear superposition of the PA pressures from all of the point sources with different delay time and attenuation. Equation (7) is more exact than the relationship given by Kruger *et al* (1995)

$$p(\mathbf{r}, t) = \frac{\beta I_0 c}{4\pi C_p}\tau\frac{\mathrm{d}}{\mathrm{d}t}\oint\int_{|\mathbf{r}-\mathbf{r}'|=ct} A(\mathbf{r}')\frac{\mathrm{d}\mathbf{r}'}{ct} \tag{8}$$

where τ is the pulse width of the laser. Equation (8) is obviously independent of the laser pulse shape.

In practice, because of the finite bandwidth of an ultrasound transducer, recorded PA signals $p_d(t)$ are the convolutions of induced PA pressures $p(t)$ and the impulse response $h(t)$ of the transducer, we can write

$$\begin{aligned} p_d(t) &= p(t) * h(t) \\ &= \frac{\beta r_p}{4\pi C_p k}\left(\frac{1}{t}\oint\int_{|\mathbf{r}|=ct} A(\mathbf{r})\,\mathrm{d}S\right) * p_0(t) * h(t) \\ &= \frac{\beta r_p}{4\pi C_p k}\left(\frac{1}{t}\oint\int_{|\mathbf{r}|=ct} A(\mathbf{r})\,\mathrm{d}S\right) * p_{d0}(t) \end{aligned} \tag{9}$$

where $p_{d0}(t) = p_0(t) * h(t)$, $p_{d0}(t)$ denotes the recorded PA signal from the point source. Equation (9) can be written as

$$\oint\int_{|\mathbf{r}|=ct} A(\mathbf{r})\,\mathrm{d}S = \frac{4\pi C_p k t}{\beta r_p}\,\mathrm{IFFT}\left(\frac{P'_d(\omega)W(\omega)}{P'_{d0}(\omega)}\right) \tag{10}$$

where $P'_d(\omega)$ and $P'_{d0}(\omega)$ are the Fourier transforms of $p_d(t)$ and $p_{d0}(t)$, respectively, and $W(\omega)$ is a window function used to band-limit the signals and taper the high-frequency components smoothly to zero (Kruger *et al* 1999). Equations (9) and (10) provide a convolution relationship between PA signals recorded by an ultrasound transducer and optical absorption distribution. Based on equations (9) and (10), the projections of optical absorption distribution can be obtained by a deconvolution algorithm in the time domain. The optical absorption distribution can be reconstructed using the filtered back projection algorithm with a sufficient number of projections acquired at different directions. As opposed to the true filtered back projection, here, back projection is carried out over spherical surfaces rather than planes. The advantage of using equations (9) and (10) for imaging is that we can easily measure $p_{d0}(t)$ by focusing the incident laser on an absorber surface to form a point absorption source and thus eliminate the need for measuring the impulse response of the transducer. Equation (6) indicates that

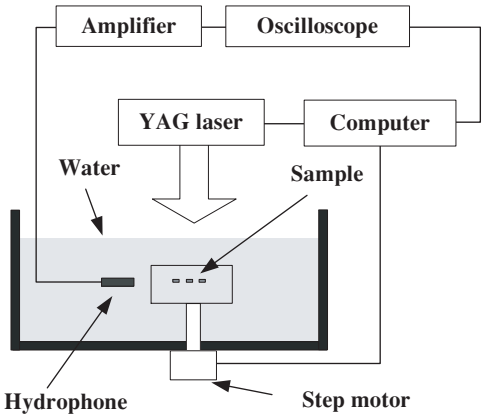

Figure 1. Experimental setup for photoacoustic imaging.

the photoacoustic pressure from a point absorption source is only dependent on the temporal function of the laser pulse, so the point absorption source can be chosen from an easily made sample. The reconstruction is accomplished by (1) calculating the projections of the optical absorption distribution according to equation (10); (2) filtering the projections using the Shepp–Logan function $R(\omega) = |\omega(2\pi)| \sin c(\omega)$; (3) back projecting it over spherical surfaces (3D) or arcs (2D) and (4) summing the back projections.

3. Methods and materials

The experimental setup for the PA imaging system is shown in figure 1. A Q-switched Nd:YAG laser operating at 1064 nm with a pulse duration of 7 ns, and a repetition rate of 30 Hz, was used as the light source. A piece of ground glass was used to homogenize the laser beam. The incident energy density of the laser beam was controlled below $\sim$20 mJ cm^{-2}. The hydrophone (Precision Acoustics Ltd) used to record PA signals had a diameter of 1 mm and a sensitivity of 950 nV Pa^{-1}. It was fixed and pointed to the centre of a rotating sample stage. The hydrophone and phantoms to be imaged were both immersed in water for better coupling of acoustic waves. Phantoms were fixed on the sample stage and rotated through 360°. PA signals were recorded every 1.8°. At each angle, the PA signals were averaged 128 times by an oscilloscope (TDS3032, Tektronix), and then the signals were transferred to a personal computer. After the 200 series of data were recorded, projections were calculated using equation (10). Images were reconstructed with the filtered back projection algorithm.

To verify equations (9) and (10), we measured the PA pressure from an absorber fabricated by embedding a thin dyed gelatine disc, 3.5 mm in diameter and 0.5 mm in height, within a transparent gelatine cylinder. The laser beam with homogeneous intensity distribution was projected normally to the disc surface. The hydrophone was positioned in the same plane of the disc and pointed to the centre of the disc. The laser beam was then focused on a 'point' on the dyed gelatine disc surface. The recorded PA signal was regarded as originating from a point source. The profile of the focused zone is adjusted to be $\sim$100 μm. It blurs the reconstructed images by $\sim$100 μm.

Then two tissue-mimicking phantoms were imaged according to the above method. A cylindrical turbid phantom made of a mixture (water = 500 ml, gelatine = 105 g and low fat milk = 100 ml) was used to simulate the optical properties of human breast. The phantom

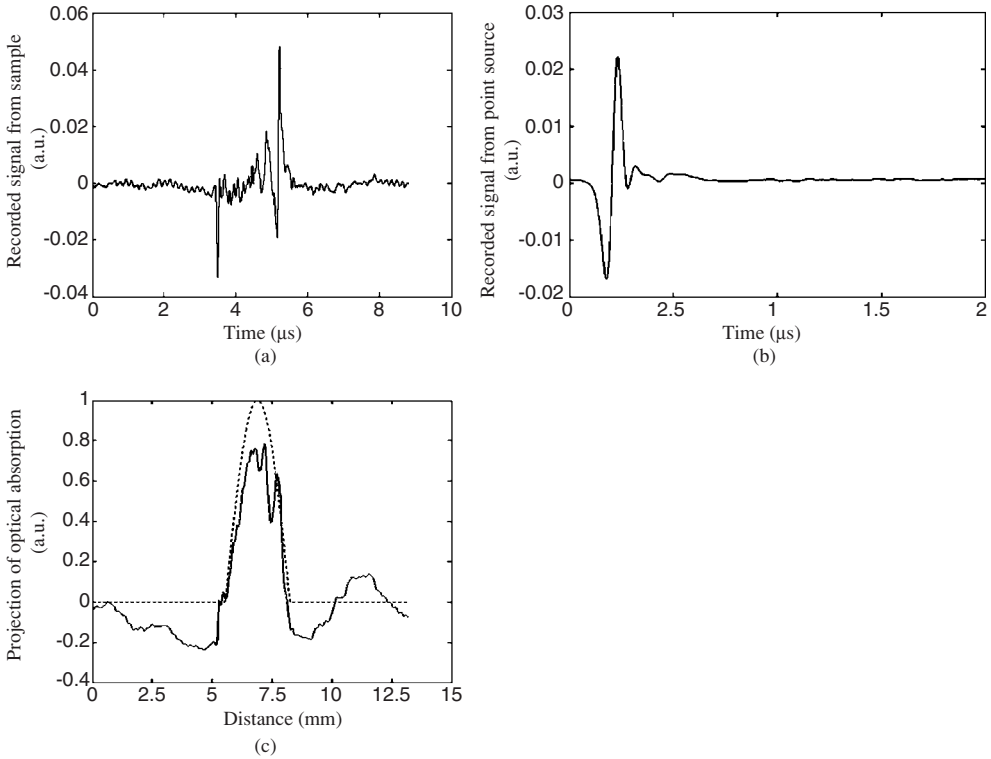

Figure 2. (a) Recorded PA signal from a thin dyed gelatine disc; (b) recorded PA signal from a point source and (c) projections of the optical absorption distribution of the thin disc calculated by equation (10) (solid curve) and the theoretical result (dotted curve).

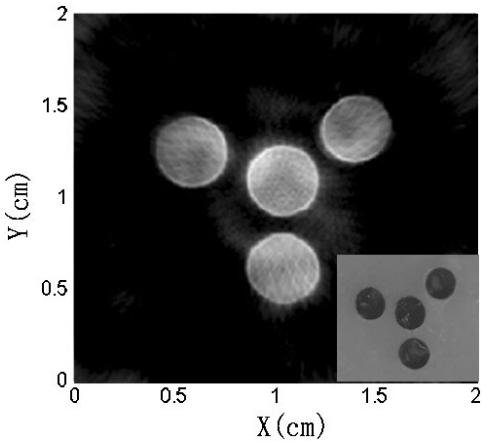

Figure 3. Reconstructed image of the four-disc phantom (inset: cross section of the phantom).

had an effective attenuation coefficient of 1.2 cm^{-1}, typical for human breast *in vivo* in the near-infrared spectral range (Larin *et al* 2001). Four thin discs with a diameter of 3.5 mm and a height of 0.5 mm made of the same mixture and a drop of dark ink were used to simulate

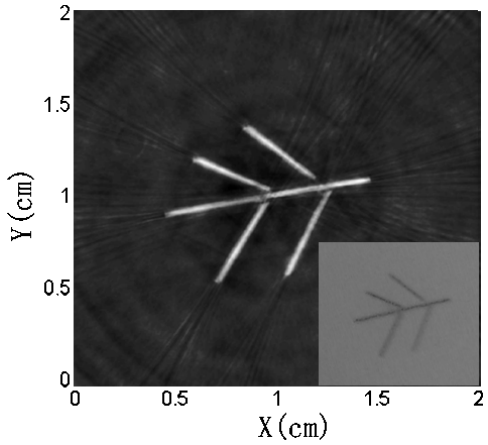

Figure 4. Reconstructed image of the five-hair phantom (inset: actual picture of the phantom).

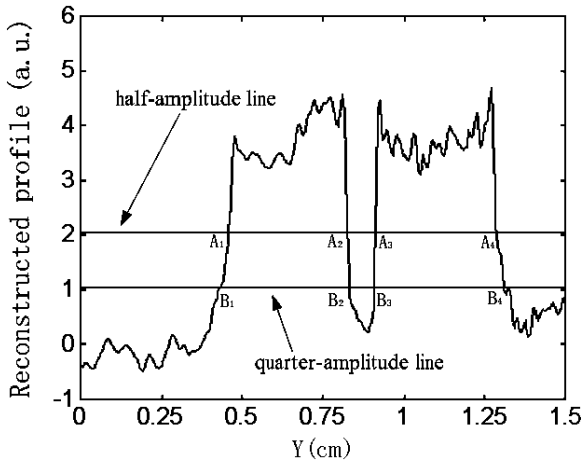

Figure 5. The line profile of the reconstructed image (figure 3) at $x = 1$ cm. The half-amplitude line and quarter-amplitude line cut across the profile at points A_{1-4} and B_{1-4}, respectively.

breast tumours with higher optical absorption. The four discs were embedded in the cylindrical breast phantom at a depth of 7 mm. Another sample was made by embedding five hairs with a diameter of 0.1 mm in a similar cylindrical turbid phantom at a depth of 7 mm, to simulate blood vessels in tissues.

4. Results and discussion

Figure 2(a) shows a typical PA signal recorded from the single-disc sample. The PA signal from the point source is shown in figure 2(b). In figure 2(c), the solid curve denotes the projection of the optical absorption distribution calculated by equation (10), and the dotted curve denotes the theoretical result $\oint \int_{|\mathbf{r}|=ct} A(\mathbf{r})\, \mathrm{d}S$. Our result agrees well with the theoretical result.

The reconstructed image of the four-disc phantom is shown in figure 3, with the cross section of the phantom shown in the inset. Figure 4 shows the reconstructed image of the

five-hair phantom, and the inset shows an actual picture of the hairs. The full width at half maximum (FWHM) of the reconstructed image of the hair is ∼0.2 mm. The reconstructed images (figures 3 and 4) are in excellent agreement with the original phantoms. It proves equations (9) and (10) to be valid for PA imaging.

Figure 5 is the profile of the reconstructed image (figure 3) at $x = 1$ cm. The profile includes two absorption sources. The half-amplitude line and quarter-amplitude line cut across the profile at points A_{1-4} and B_{1-4}, respectively. The spatial resolution of the imaging system is estimated according to the resolution criterion defined in the literature (Xu and Wang 2002). The two sources can no longer be clearly distinguished when point B_2 touches B_3. The minimum distance that the two sources can be differentiated is approximately equal to the summation of $|A_2B_2|$ and $|A_3B_3|$. We have checked additional pairs of sources in the reconstructed image (figure 3) according to the above method, and found that the maximum distance is 0.3 mm. So the spatial resolution of the imaging system reaches 0.3 mm.

5. Conclusion

A convolution relationship between laser-induced PA pressures and optical absorption distribution of a sample is given by equation (7). This relationship indicates that an absorber can be separated into a collection of point sources, and the PA pressures from the absorber are the linear superposition of the PA pressures from all of the point sources with different delay time and attenuation. Strictly speaking, this is accurate only for a point transducer, which is omnidirectional. In practice, this relationship is also appropriate for the transducer with a small aperture. In addition, equation (7) reveals that the induced PA pressure is partially dependent on the shape of the irradiating laser pulse. Moreover, equation (9) demonstrates that the PA signals recorded by a transducer from a sample can be expressed as the convolutions of the projections of the optical absorption distribution of the sample and the PA signal recorded by the same detector from a point source. Thus, the projection of the optical absorption distribution can be obtained directly by deconvolving the recorded PA signal originating from a point source out of that from the sample. The advantage of this method is that the need to know the impulse response of the transducer is eliminated and the PA signal from a point source can be easily obtained.

Karabutov *et al* (2000) and Xu *et al* (2002) have presented a similar convolution relationship, $p_I(t) = p_p(t) * I(t)$, where $p_I(t)$ is the PA pressure induced by a laser pulse with a temporal illumination function of $I(t)$ and $p_p(t)$ is the PA pressure induced by a laser pulse with a temporal illumination function of $\delta(t)$. Theoretically, it is equivalent to the relationship shown as equation (7). But, by replacing the measurement of the impulse response with measurement of the PA pressure originating from a point source, our method is more practicable for PA imaging.

Experiments demonstrate that the reconstructed images agree well with the original phantoms. The spatial resolution of the system reaches 0.3 mm. It proves the presented method to be valid for PA imaging.

Acknowledgments

This study was supported by the National Major Fundamental Research Project of China (2002CCC00400), the National Natural Science Foundation of China (60378043) and Research-Team Project of the Natural Science Foundation of Guangdong Province (015012).

References

Callasso I G, Craig W and Diebold G J 2001 Photoacoustic point source *Phys. Rev. Lett.* **86** 3550–3

Esenaliev R O, Karabutov A A and Oraevsky A A 1999 Sensitivity of laser opto-acoustic imaging in detection of small deeply embedded tumours *IEEE J. Sel. Top. Quantum Electron.* **5** 981–8

Hoelen C G A, Mul F F M, Kolkman R G M and Dekker A 1998 Three-dimensional photoacoustic imaging of blood vessels in tissue *Opt. Lett.* **23** 648–50

Karabutov A A, Savateeva E V, Podymova N B and Oraevsky A A 2000 Backward mode detection of laser-induced wide-band ultrasonic transients with optoacoustic transducer *J. Appl. Phys.* **87** 2003–14

Kruger R A, Liu P, Fang Y R and Appledorn C R 1995 Photoacoustic ultrasound (PAUS)-reconstruction tomography *Med. Phys.* **22** 1605–9

Kruger R A, Reinecke D R and Kruger G A 1999 Thermoacoustic computed tomography—technical considerations *Med. Phys.* **26** 1832–7

Larin K, Hartrumpf O, Larina I and Esenaliev R 2001 Comparison of optoacoustic tomography with ultrasound and x-ray imaging for breast cancer detection *Proc. SPIE* **4256** 147–53

Oraevsky A A, Andreev V A, Karabutov A A, Fleming D R, Gatalica Z, Singh H and Esenaliev R O 1999 Laser opto-acoustic imaging of the breast: detection of cancer angiogenesis *Proc. SPIE* **3597** 352–63

Wang X, Pang Y, Ku G, Xie X, Stoica G and Wang L V 2003 Noninvasive laser-induced photoacoustic tomography for structural and functional *in vivo* imaging of the brain *Nature Biotechnol.* **21** 803–6

Xu M and Wang L-H 2002 Time-domain reconstruction for thermoacoustic tomography in a spherical geometry *IEEE Trans. Med. Imaging* **21** 814–22